Life Sciences 230 (2019) 76–83

Contents lists available at ScienceDirect

Life Sciences

journal homepage: www.elsevier.com/locate/lifescie

Long-term biodistribution and toxicity of curcumin capped iron oxide nanoparticles after single-dose administration in mice

Nihal Saad Elbialy[a,b,*], Samia Faisal Aboushoushah[a], Wafa Wuqayyan Alshammari[c]

[a] Medical Physics Program, Department of Physics, Faculty of Science, King Abdulaziz University, Jeddah 21589, Saudi Arabia
[b] Department of Biophysics, Faculty of Science, Cairo University, Egypt
[c] Faculty of Applied Medical Science, Hail University, Hail, Saudi Arabia

ARTICLE INFO

Keywords:
Curcumin capped iron oxide nanoparticles
Biodistribution
Clearance
Toxicity
Serum biochemical analysis

ABSTRACT

Aim: In this study, in vivo biodistribution, clearness and toxicity of curcumin capped iron oxide nanoparticles (Cur-IONPs) were addressed in different body organs.
Materials and methods: The physicochemical properties of the prepared Cur-IONPs were investigated. Long term (3 weeks) biodistribution, clearness and toxicity were assessed for a single-dose administration of Cur-IONPs (5 mg/kg). The iron content in liver, kidney, spleen and brain was quantified using atomic absorption spectroscopy. Serum biochemical parameters were also measured.
Key findings: The integrated in vivo results demonstrated that Cur-IONPs was mostly taken up in the liver and spleen reaching its highest levels on days 1 and 2, respectively. In the brain, the results showed significant accumulation of Cur-IONPs between 1 h to 1-day post injection. This represented the successful penetration Cur-IONPs across the blood-brain barrier. Serum biochemical analysis demonstrated a temporal disturbance in the performance of body organs. Also, the body weights showed no alteration throughout the experiment.
Significance: It has been deduced that the promising green synthesized Cur-IONPs as an "All in One" nanoplatform is safe enough to be used in diagnostic and therapeutic purposes.

1. Introduction

An essential task of nanomedicine is designing non-toxic, biocompatible and multifunctional nanoformulations. The development and production of newly manufactured nanomaterials have grown much faster than the generation of sufficient toxicological information. The toxicological behaviour of materials at the nanoscale is far beyond predictions of what is known at the macro and bulk scale of the same material [1]. Therefore, it is necessary to assess the toxicity of the manufactured nanomaterials, even though the toxicity of the bulk material with the same chemical composition might already be known.

Many researchers have elucidated the possibility of detrimental biological effects due to the administration of nanomaterials [2,3]. However, the exact effects of these nanomaterials on human health and the environment remain unclear [4–6]. One of the main concerns is to determine the interactions of different types of nanoparticles (NPs), as a function of their shape, size and surface modifications, with biological cells [7,8]. This has led to the emergence of "Nanotoxicology" as an independent field of research, that provides data regarding the toxicity of nanoparticles.

Literature data screening, of research performed during this decade, has shown that the biodistribution and toxicity of nanoparticles has become an issue of concern [9–14]. At the cellular level, NPs may induce many adverse effects by interacting with the cell membrane, mitochondria, or nucleus. These effects cause organelle or DNA damaging, oxidative stress, programmed cell death, change in protein regulation, and mutagenesis [15–17].

Up until now, only fragmentary data explaining the biological mechanisms governing NPs cytotoxicity has been reported. In these studies, numerous factors that affect nanotoxicity including: particles size [18–22], surface charge [23–28] and surface modification [29] have been demonstrated.

Most in vitro studies demonstrate that NPs with a size of 10–60 nm show a marked cellular uptake, regardless of core composition or the surface charge of the nanomaterial [18,19]. Interestingly, it has been found that the nanomaterial size plays an important role not only in the cellular interaction and uptake, but also extends to in-vivo pharmacokinetics, biodistribution and the circulation half-life of NPs, which in

* Corresponding author at: Medical Physics Program, Department of Physics, Faculty of Science, King Abdulaziz University, Saudi Arabia. Biophysics Department, Faculty of Science, Cairo University, Egypt.
E-mail addresses: nsmohamad@kau.edu.sa (N.S. Elbialy), aboushoushah@kau.edu.sa (S.F. Aboushoushah).

https://doi.org/10.1016/j.lfs.2019.05.048
Received 13 April 2019; Received in revised form 13 May 2019; Accepted 19 May 2019
Available online 22 May 2019
0024-3205/

turn leads to different biological effects. For biomedical applications, the optimal size of the nanomaterial depends on the specific targeted tissue. The size-dependent organ distribution of nanomaterials has been investigated [30], and it was reported that some nanomaterials with a hydrated diameter lower than 10 nm are rapidly removed by the kidneys through renal filtration, which has an effective cut-off size of about 10 nm. On the other hand, NPs with a diameter > 150 nm are removed from circulation and accumulated in the spleen and liver [20]. Sun, et al. [21], found that at 1 h post administration of 24 and 37 nm polymeric nanoparticles, 50% of the small diameter nanomaterial was found in the blood stream, compared with only 5% of the larger one. Another study, demonstrated that pegylated gold nanomaterial with a core size of 17 nm exhibited an eight-fold increase in circulation half-life time in comparison with that of a core size of 86 nm [22].

The surface properties of NPs may also be crucial to their cytotoxic effect [23]. It was found that positively charged nanoparticles disrupt the cellular membrane's negative charges by electrostatic interactions [24]. Also, Uboldi, et al. [25] suggested that the residue of sodium citrate adsorbed on NPs surface was responsible for cytotoxicity. Furthermore, it was reported that the citrate-capped NPs stimulate the macrophages respiratory activity and the activity of enzymes for mitochondrial macrophage [26]. Sun, et al. [27], found that, not only the type of surface coating affects the nanotoxicity, but that also, by increasing the concentration of adsorbed molecules on the NPs surface would cause a decrease in the survival of HeLa cells. In fact, NPs endocytosis depends on their surface chemistry. For a size range 10 to 100 nm, coated iron oxide cannot be easily filtrated by the reticuloendothelial system and has a long circulation time, whereas uncoated iron oxide tends to aggregate in biological fluids, resulting in rapid removal from blood circulation [28].

Additionally, NPs' surface modification plays a critical role in the interaction between nano-formulations and the biological system. Applying a shell to the surface of NPs improves their biocompatibility and solubility in water and other biological fluids. In this manner the shell decreases the toxicity of NPs and supplies them with the facility for selective interactions with different types of biological systems. The shell also improves NPs stability, expands their opposition to environmental factors and minimizes the release of toxic substances from their core [29].

Iron Oxide Nanoparticles (IONPs) offer promising possibilities in the nanomedical field mainly due to their physicochemical properties and magnetic features [31,32]. Applications include: cell separation, contrasting agents for magnetic resonance imaging, cell labelling, drug delivery and magnetic hyperthermia [11,13,33–35]. Some studies have reported the high biocompatibility and none-to-low toxicity of IONPs [14,36,37]. While other studies have reported contradictions to this [1,38], revealing that NPs may cause significant genotoxicity, biochemical alterations and oxidative stress. It is thus of high importance for further research to be conducted to assess the toxicity of NPs in general and specifically IONPs. IONPs are also prone to the body's highly active clearance mechanism consequently limiting their biodistribution [39,40]. Recent progress in synthesis, characterization and surface modification of the IONPs has enabled researchers to improve the bioavailability parameters of IONPs in biological applications [41,42]. In particular, green chemistry has become a new approach for the synthesis of eco-friendly, biocompatible metallic nanoparticles using natural compounds rather than organic chemical substances [12,43,44]. One such natural product is curcumin (CUR), which is a nutraceutical compound isolated from the rhizomes of the herb *Curcuma longa*. CUR has received considerable attention due to its multiple biological activities including anti-microbial, anti-inflammatory, anti-oxidant, anti-cancer activities and wound healing [45]. CUR is also a "Generally Recognized as Safe" compound by the Food and Drug Administration (FDA).

The green synthesis of iron oxide nanoparticles may be performed using prokaryotic, eukaryotic, microorganisms, or plant extracts [46,47]. The bio-molecules act as reducing agents to promote the reduction of metal atoms resulting in the formation of nanoparticles. At the same time these biomolecules act as a stabilizing layer (coating) on the surface of nanoparticles, preventing them from aggregating or growing in a disorderly manner during their production. Most of the IONPs obtained from green synthesis show desirable properties: (1) eco-friendly (use of lesser toxic reagents and solvents), (2) simple and rapid synthesis procedures (few steps), (3) biocompatible (can be used directly without purifications), (4) biodegradable (can be hydrolyzed by biological pathways), and (5) economically efficient (low production cost) [12].

Based on the above discussion, the size, surface coating and/or shape of nanomaterial need to be tailored in a specific manner so as to gain the best advantage of the unique properties of IOPNs, which can then be utilized for different biomedical applications.

Accordingly, in this study, we attempted to minimize the toxicity of the IONPs using an eco-friendly approach. The aim of this work is the green synthesis of IONPs using the medicinal plant curcumin to enhance the biosafety profile of the prepared nanoformulation. It is expected that curcumin capped iron oxide nanoparticles will exhibit high stability as well as high degree of safety enabling its potential utilization in different biomedical applications. In order to verify this, the in-vivo biodistribution and toxicity of curcumin capped iron oxide nanoparticles (Cur-IONPs) will be studied.

2. Materials and method

2.1. Materials

Iron (II) chloride ($FeCl_2{\cdot}4H_2O$), iron (III) chloride hexahydrate ($FeCl_3{\cdot}6H_2O$), ammonium hydroxide (NH_4OH), nitric acid (HNO_3), curcumin powder, ketamine/xylazine (KX) and phosphate buffered saline (PBS) were purchased from (Sigma- Aldrich, USA). Dimethyl sulfoxide (DMSO) was purchased from Gibco (USA). Biochemical analysis kits for Creatinine (Cr), Uric Acid (UA), urea, alanine aminotransferase (ALT), and aspartate aminotransferase (AST), albumin were purchased from BioMed Diagnostic (Singapore).

2.2. Methods

2.2.1. Green synthesis of Iron oxide nanoparticles coated with Curcumin

Cur-IONPs were synthesized as described [48]. An aqueous solution of Fe (III) and Fe (II) salts with a molar ratio of (2:1) was dissolved in 40 ml of water and stirred for 15 min at 40 °C till the appearance of a brown colour. Then, 100 μl of curcumin solution (20 mg curcumin dissolved in 1 ml DMSO) was added to the mixture drop-wise. The mixture was heated and 5 ml of 28% ammonium hydroxide was added, till the mixture's colour turned black. The mixture was left to cool till a black precipitate was seen topped by a clear transparent supernatant.

In order to measure curcumin loading efficiency, the supernatant was removed using a pipette and then optically measured using an UV–visible spectrophotometer. The precipitate was washed and dried, completing the formation of Cur-IONPs.

2.2.2. Physicochemical characterization

Cur-IONPs were characterized using: Transmission Electron Microscope (TEM), Zeta Potential, Vibrating-Sample Magnetometer (VSM), UV-VIS-IR spectroscopy and X-ray diffraction (XRD).

2.2.2.1. TEM. Cur-IONPs size and morphology were visualized by TEM (HR-TEM, Tecnai G20, FEL, Netherland) at an electron acceleration voltage of 200 kV.

2.2.2.2. Zeta potential measurements. The surface potential of Cur-IONPs was determined using the Zeta Potential/Particle Seizer [Malvern, UK, Zeta sizernano series (Nano ZS), 0.6:6000 nm,

operating at (−200:200 mV)]. The measurements were repeated three times and the standard deviation (SD) was calculated using origin 8.0 software.

2.2.2.3. VSM. The magnetic properties of Cur-IONPs were investigated using VSM (LakeShore 7410, LakeShore, and Westerville, USA).

2.2.2.4. UV-VIS-IR spectroscopy. The absorbance spectrum of Cur-IONPs was measured using UV-VIS-IR Spectroscopy.
(Jenway 6405, Barloworld Scientific, Essex, UK).

2.2.2.5. X-ray diffraction (XRD). X-ray diffraction (XRD) technique was used to measure the diffraction pattern of Cur-IONPs using the XPERT-PRO-PAN analytical, Nether land (operating at 45 kV and 30 mA) with a CuKα radiation (k = 1.54056 Å). The sample was scanned from 5 to 70.

2.2.3. In vivo studies

The study protocol met the approval conditions of the Unit of Biomedical Ethics Research Committee (registration No. HA-02-J-008, reference No.76-17, 13/03/2017) at King Fahad Medical Research Centre (KFMRC).

2.2.3.1. Animals. Forty-five male Balb/c mice with a weight of 25–28 g were obtained from the KFMRC, King Abdulaziz University. The animals had access to food and water, and were kept at a facility with a 12-hour light/dark cycle with controlled humidity and temperature.

2.2.3.2. Single dose administration. The objective of this protocol was to assess the biodistribution and toxicity of a single Cur-IONPs dose at different time points (0.5 h, 1 h, 2 h, 1 day, 2 days, 1 week, 2 weeks, 3 weeks) following the administration. Mice were divided into 9 groups (n = 5). Mice in the control group received an intravenous (IV) injection of 100 μl phosphate buffered saline (PBS). The remaining 8 experimental groups received 100 μl Cur-IONPs of (5 mg/kg) via the tail vein.

For serum biochemical analysis, blood samples were collected from the control and the treated groups at the designated time points, as mentioned above. Blood was withdrawn from the Orbital Sinus. Serum fractions were immediately separated by centrifugation at 2000 rpm for 15 min and stored at −80 °C till the end of the experiment. The mice were then sacrificed using an over dose of anesthesia ketamine/xylazine mixture (87/13 mg/kg) at the designated time points. The four organs (liver, kidney, spleen, and brain) were collected form mice of each group (n = 5) and stored at −80 °C until the measuring of their iron content using atomic absorption spectroscopy (AAS) was performed.

i) Serum Biochemical Analysis

Blood samples were collected at the appointed time points from Cur-IONPs treated groups as well as the control group. Serum biochemical analysis was conducted to assess the performance of liver and kidney. Aspartate transaminase (AST) and alanine transaminase (ALT) were measured to evaluate liver function. The levels of uric acid (UA), albumin, urea, and creatinine (CRE) were measured to assess kidney function. The total iron content in the serum was measured to investigate the effect of the administrated magnetic nanoparticles on blood constituents. Additionally, the glucose (Glc) level was measured.

All measurements were performed according to the procedures of the biochemical kit assay.

ii) Atomic Absorption Spectroscopy

To study the biodistribution of Cur-IONPs in the four body organs, the organs were weighed and digested overnight with 2 ml of 70% nitric acid: 36% hydrochloric acid (1:1 v/v) at 70 °C. The solution was diluted with deionized water to a final volume of 10 ml and filtered through a 0.2 μm polyethersulfone (PES) filter. The samples were then analysed using AAS.

iii) Body Weight Measurements

Mice body weight was measured twice weekly throughout a period of three weeks.

2.2.4. Data analysis and statistics

All data was calculated and displayed as an average ± SE. The p-values *p ≤ 0.05, **p ≤ 0.01 and ***p ≤ 0.001 were considered statistically significant relative to the control group. Data was compared by one-way analysis of variance (ANOVA) using Fisher's LSD (least significance difference). Statistical analysis was performed using the statistical package SPSS.

3. Results

3.1. Physicochemical characterization

TEM images revealed the successful preparation of Cur-IONPs. Cur-IONPs appeared mono-dispersed, spherical in shape, with an average size > 10 nm, as shown in Fig. 1.a. This would potentially facilitate high cellular uptake of Cur-IONPs by human endothelial cells [49].

The measured Zeta potential of Cur-IONPs was −35 ± 2.5 mV (Fig. 1.b). Such a high negative value indicates the non-aggregate nature of the prepared Cur-IONPs. The negative charge value greatly minimizes the tendency of nanoparticles to absorb plasma proteins, thus providing Cur-IONPs stability and prolonging its blood circulation time, [50].

The measured magnetic parameters of Cur-IONPs using VSM were 87.419 E-3 emu/cm^3, 18.975 G and 3.2237E-3 emu/cm^3 for magnetization saturation (Ms), magnetic coercivity (Hci) and Retentivity (Mr) respectively (Fig. 1.c). As shown in (Fig. 1.c) the hysteresis curve with high Ms value demonstrated the small size and the superparamagnetic behavior of Cur-IONPs. Moreover, there is no observed hysteresis loop as indicated by the small value of Hci. The small values of coercivity and remanence of the hysteresis loop further confirm the superparamagnetic property of Cur-IONPs, [51]. This in turn extends the biomedical applications of Cur-IONPs. The superparamagnetic property of Cur-IONPs plays an important role in targeted drug delivery to the diseased site via an external magnetic field. Upon the removal of the magnetic field, the nanoparticles will aggregate and can escape successfully from phagocytes achieving a prolonged circulation time [52]. Furthermore, the green synthesized Cur-IONPs act as nanocarriers for the medicinal plant curcumin. Additionally, superparamagnetic iron oxide nanoparticles (SPION) can be used as a contrast agent providing highly sensitive magnetic resonance imaging for early tumor detection. Accordingly, the promising Cur-IONPs can potentially be used either as therapeutic or diagnostic agents.

As shown in Fig. 2a, there is no absorption peak for Cur-IONPs in UV-VIS-IR range (200–800 nm), which in agreement with previous study by Ghorbani et al. 2018 [50].

In Fig. 2b, XRD pattern of Cur-IONPs showed characteristic peaks at 2θ = 30.2, 35.5, 43.2, 53.6, 57, 62.75. It is obvious that the diffraction peaks of Cur-IONPs were consistent with the typical diffraction peaks of Fe_3O_4 reported in previous studies [53,54]. This consistency indicated that the fabrication of Cur-IONPs has no effect on Fe_3O_4 crystalline structure.

Measurement of curcumin loading efficiency showed that the total amount of curcumin loaded on iron oxide nanoparticles was about 96%.

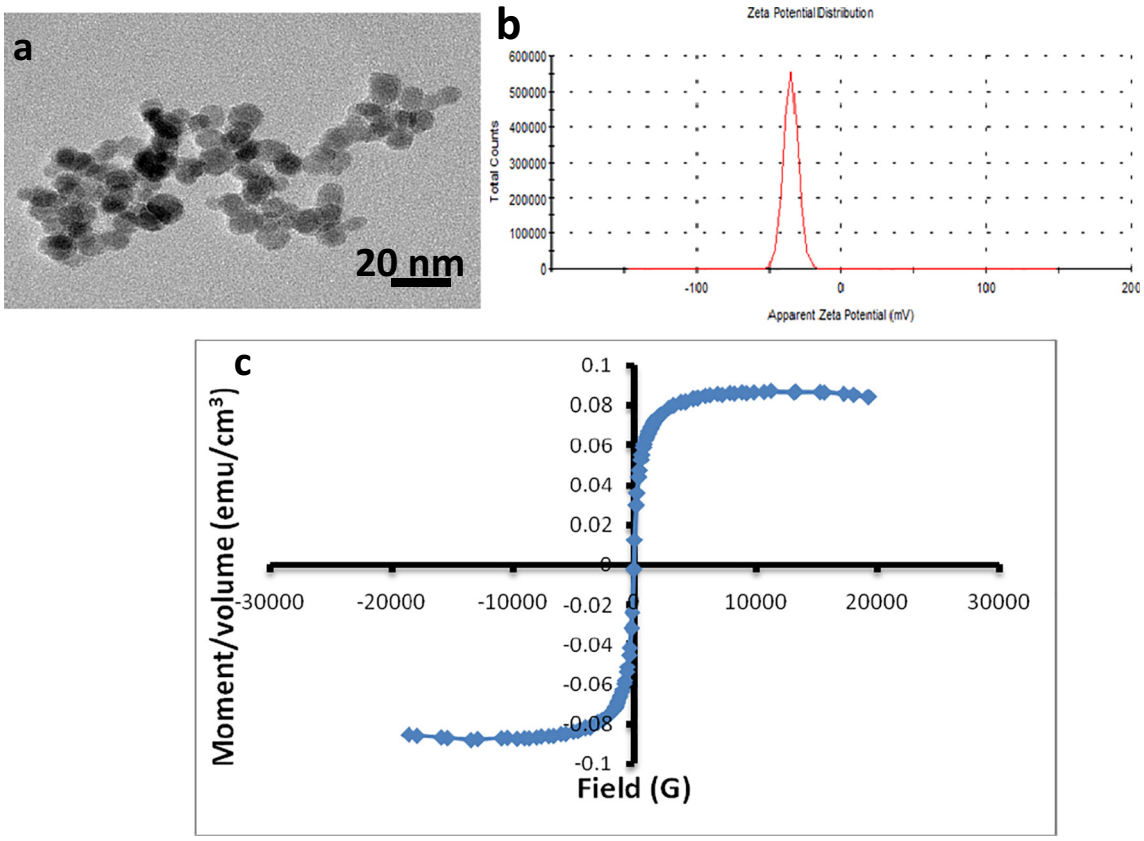

Fig. 1. Cur-IONPs (a) TEM images. (b) Zeta potential measurement. (c) Magnetization profile performed by VSM.

3.2. *In vivo studies: single dose administration*

3.2.1. *Biodistribution of Cur-IONPs*

Liver iron content for the treated groups started increasing 0.5 h post injection reaching the maximum (7-fold increase) at day-1 post injection. By the end of week-1 iron content had returned to the normal level as in the control group (Fig. 3.a).

Kidney iron content exhibited no significant change between the treated and control groups (Fig. 3.b).

Spleen iron content started increasing 1 h post injection reaching a two-fold increase on day-2 followed by a gradual decrease compared with the control group (Fig. 3.c).

Brain iron content began increasing 1 h post injection reaching the maximum (2-fold increase) at 2 h post injection relative to the control group, then returning to the normal level 2 days post injection (Fig. 3.d).

The maximum accumulation of iron in the liver, spleen, kidney and brain was at day-1, day-2, 2 h and 2 h respectively. The iron content in the liver was the greatest followed by the spleen then the kidney and then the brain (273.81 ± 10.57 μg/g, 155.45 ± 37.25 μg/g, 58.70 ± 3.3 μg/g and 44.55 ± 2.85 μg/g, respectively). This reveals the varying biodistribution of Cur-IONPs in different body tissue.

Our results showed a relevant relationship between the iron concentration changes in blood and the iron tissue content in the liver, kidney, spleen and brain. A large number of Cur-IONPs were collected by mononuclear macrophages in the liver or spleen after being injected intravenously. Consequently, Cur-IONPs concentration represented by the iron content in the liver and spleen reached their highest levels on days 1 and 2, respectively, this is in agreement with [55,56]. The marked accumulation of iron in liver tissues is attributed to the ability of hepatocyte to detoxify Cur-IONPs as ferritin or hemosiderin [57]. Our results are also in agreement with Pham et al. [58], where the maximum accumulation of IONPs in the liver was at 4 h post injection and the clearance was between 48 h–1 week. Owing to the very small size of the Cur-IONPs > 10 nm, the content of iron in the kidney remained slightly above the background level throughout the time intervals of the experiment indicating that the iron renal excretion was modest [56].

Interestingly, the results demonstrated that the accumulation of Cur-IONPs in brain tissues was time dependent, this is in accordance with the results of Nosrati et al. 2019 [35]. There was a significant difference between brain iron content of the treated and control groups. This indicated the successful penetration of Cur-IONPs across the blood–brain barrier (BBB). The biodistribution pattern of Cur-IONPs in the brain may be influenced by the iron binding proteins: transferrin and ferritin that enable iron uptake by body organs. Accordingly, the increased iron content in brain tissues could be attributed to the stimulation of iron receptors in the brain due to the effect of iron transferrin binding [58]. Furthermore, the small nanoparticle size of the promising Cur-IONPs facilitated their passage across the BBB and the incorporated curcumin increased the biocompatibility of the nanoparticle [59–61].

3.2.2. *Toxicity assessment (serum biochemical analysis)*

Serum Biochemical Parameters of Liver: Measuring the level of the enzymes; AST, ALT and albumin can assess the proper performance of the liver. Compared with control group, AST activity started to increase 0.5 h post injection, reaching the maximum value (2-fold increase) 1-week post-injection. During week 2 and 3, the serum AST level began decreasing while still showing a significant difference compared with the control group (Table 1). Similarly, ALT activity started increasing 0.5 h post-injection reaching its maximum at week 1, then it began gradually decreasing until week 3 (Table 1). While, the serum albumin level revealed a significantly high increase 2 h post injection and then returned back to normal after day 1 (Table 1).

The significant high levels of AST and ALT are attributed to the

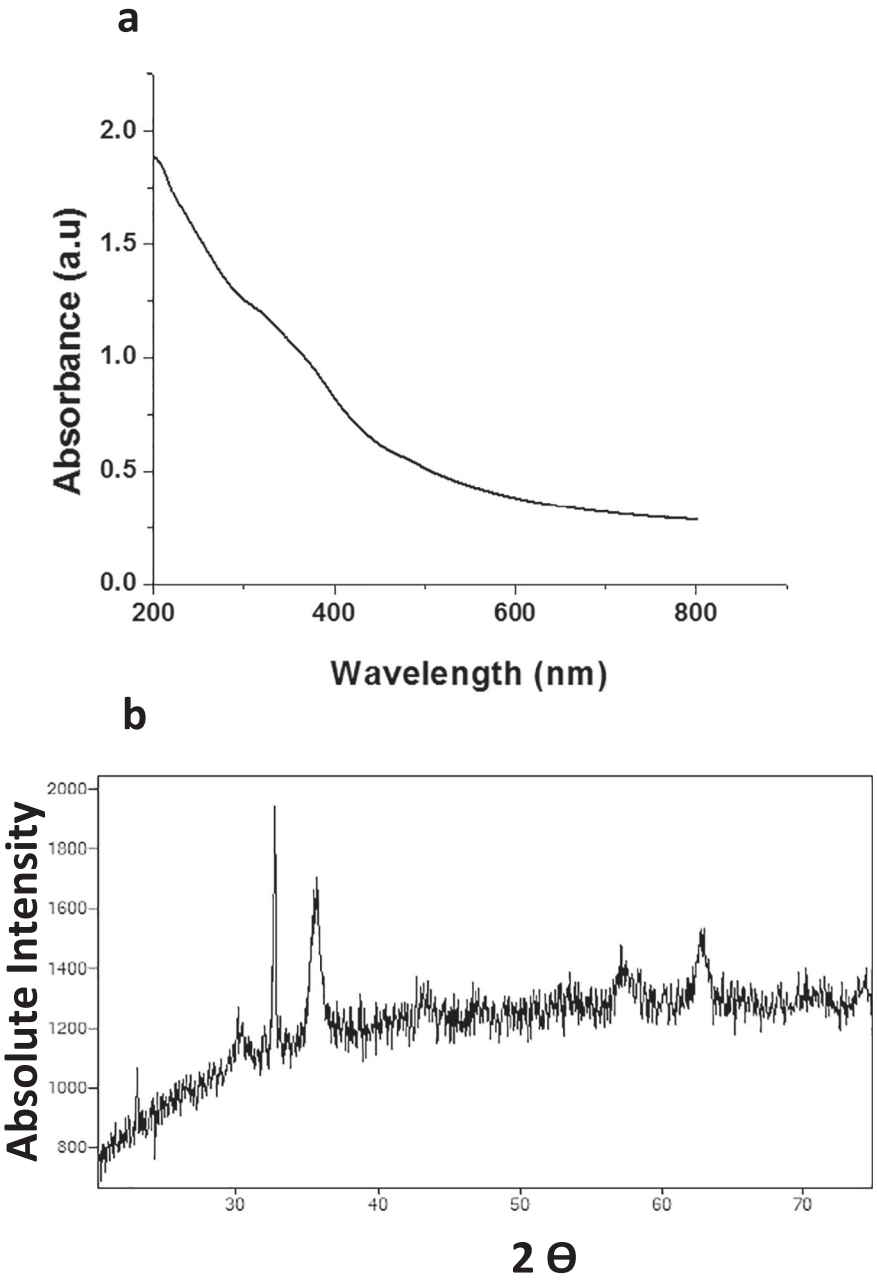

Fig. 2. (a) UV-VIS-IR spectrum of Cur-IONPs. (b) XRD pattern of Cur-IONPs.

uptake and accumulation of nanoparticles by hepatocytes and Kupffer cells, which are special macrophages located in the liver [62]. These results are in agreement with Wei et al. [63], where the levels of AST and ALT increased 24 h post magnetic nanoparticles injection than declined throughout the following two weeks. These findings are in contrast to Storey et al. [64], as a prolonged retention of nanoparticles in body organs (11 months) was noticed. In the present study, it was clearly observed that Cur-IONPs retention in the four body organs was limited to a certain time period, indicating that the promising Cur-IONPs causes minimum cytotoxicity. The transient increase in AST and ALT levels in serum upon administration of Cur-IONPs might be attributed to the normal response of mice to blood withdrawal. In addition to, the anesthesia that may stimulate the liver activity and in turn increases liver enzymes level. In a similar study, Jiang et al. [65], a transient increase in ALT and AST activity following injection of chitosan- and polyethylenimine-DNA complexes was observed. Generally, AST levels three times the upper limit of the normal range (range 39–262 U/l) represent abnormal liver function [66]. The results in this study are consistent with Jain et al. [66], where liver enzymes disturbance was only confined to a certain time interval. This demonstrates the safety of Cur-IONPs when being used as a drug nanocarrier and image contrast agent.

Serum Biochemical Parameters of Kidney: The levels of serum urea, CRE and UA in the blood are associated with the functionality of the kidney. For the treated groups, the serum urea level increased reaching its highest value at 1 h post injection, after which, it decreased to its normal level one day post injection (Table 1). The serum CRE level showed a significant increase ($p < 0.001$) at 2 h post injection compared with the control group. By 1-week post injection, the CRE level had returned back to its normal level (Table 1). The serum level of UA showed a significant increase after 0.5 h followed by a rapid decrease returning back to normal level (Table 1).

The performance of the kidney, represented by the levels of serum urea, CRE and UA, revealed temporal variations in the treated groups

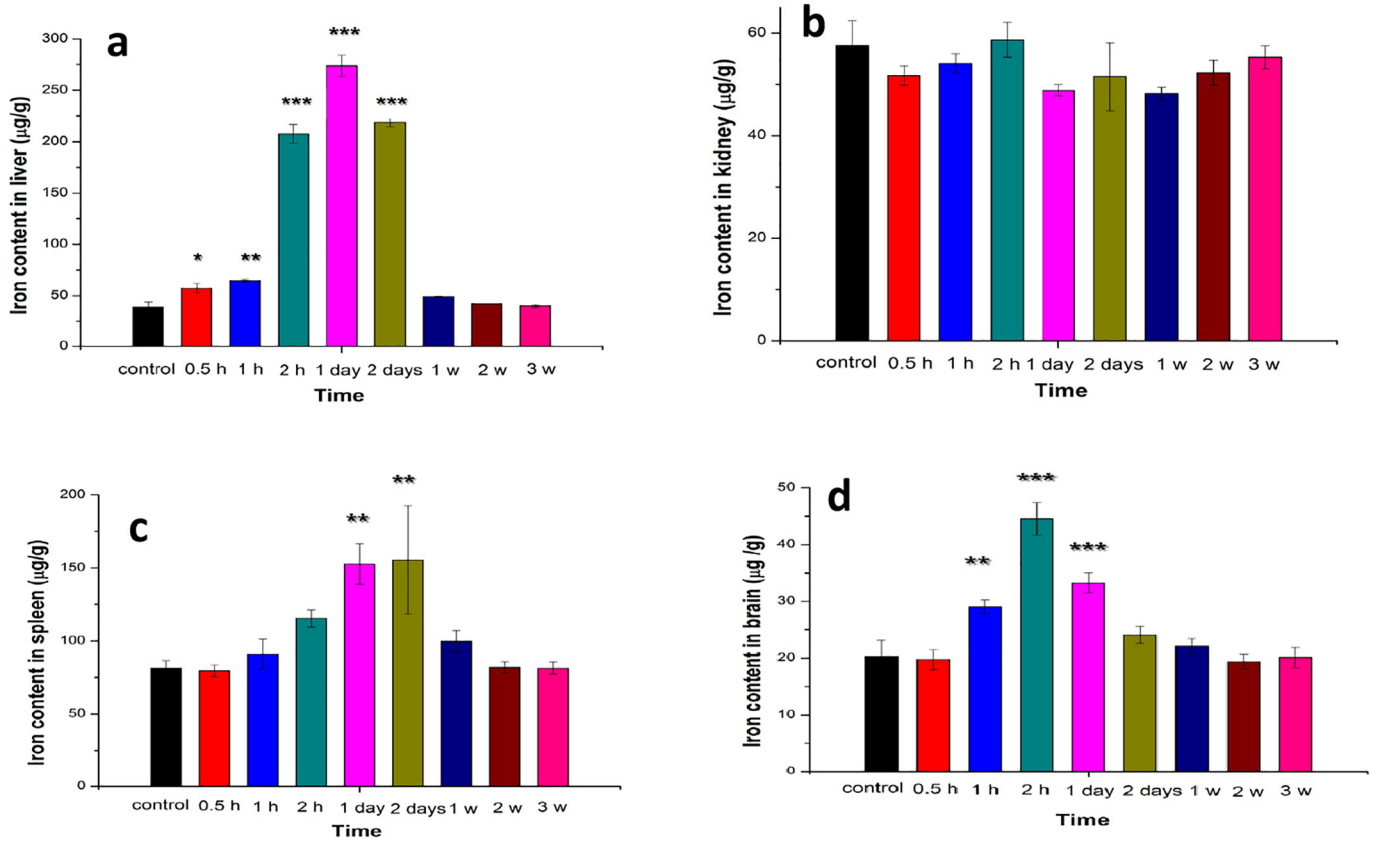

Fig. 3. Iron content for the control group and Cur-IONPs treated groups, over the time intervals (0.5 h, 1 h, 2 h, 1 day, 2 days, 1 week, 2 weeks, and 3 weeks). In (a) the liver, (b) the kidney, (c) the spleen, and (d) the brain. Data represents mean ± SE (n = 5).

compared with the control group. However, these observed changes might be attributed to the ultra-small size of Cur-IONPs that provides rapid clearance from kidney tissues (Table 1).

Blood Glc Level: All groups showed a significant decrease in blood sugar level except for the 1-week group, which showed a significant increase in blood sugar concentration in comparison with the control group (Fig. 4a). Therefore, it cannot be excluded that Cur-IONPs might induce temporal inflammation in pancreatic cells resulting in a high glc level during week-1 post injection. However, in the following two weeks the glc level returned to its normal level (Fig. 4a).

Serum Iron Concentration: Compared with the control group, the serum iron level started to increase 0.5 h post injection and exhibited a significant increase throughout the first two weeks. Thereafter, the serum iron level began to decline slowly returning to its normal level after 3 weeks (Fig. 4b). In this study, serum iron data was only concerned with the free iron forms and not with its bound one. The extended high iron level over a period of 2 weeks indicated the rate of iron clearance from the body. These results are consistent with the study of Bourrinet et al. [67] that showed 7 weeks clearance. This might be due to the incorporation of the injected iron into the stored body iron, which in turn slows down its clearance. However; Jain et al. [65] reported rapid iron clearance from the body. This discrepancy in iron clearance time is owed to the differences in the size and surface coating of the synthesized iron oxide nanoparticles, which can greatly affect its biodistribution and clearance.

Table 1
The serum concentration of: AST, ALT, Albumin, urea, CRE and UA measured over the time intervals (0.5 h, 1 h, 2 h, 1 day, 2 days, 1 week, 2 weeks, and 3 weeks) for control and treated groups.

Test	AST(U/l)	ALT(U/l)	Albumin(gm/dl)	Urea (md/dl)	CRE (md/dl)	UA (md/dl)
Control	161.00 ± 8.50	39.50 ± 2.50	2.10 ± 0.07	32.33 ± 1.76	0.33 ± 0.02	2.80 ± 0.15
½ h	256.33 ± 16.29***	84.33 ± 1.20***	2.47 ± 0.23	50.00 ± 5.51**	0.48 ± 0.02**	3.40 ± 0.25*
1 h	295.00 ± 2.65***	85.33 ± 0.88***	1.70 ± 0.15	50.67 ± 5.90**	0.53 ± 0.03***	2.50 ± 0.17
2 h	264.00 ± 6.67***	96.00 ± 1.53***	2.80 ± 0.06**	45.00 ± 2.65*	0.63 ± 0.03***	3.00 ± 0.12
1 day	251.00 ± 12.22***	104.00 ± 3.06***	2.53 ± 0.19	33.25 ± 2.53	0.48 ± 0.02**	2.95 ± 0.06
2 days	272.00 ± 12.29***	136.00 ± 10.15***	2.20 ± 0.21	25.00 ± 2.65	0.50 ± 0.06**	2.83 ± 0.29
1 week	371.33 ± 6.39***	208.33 ± 18.52***	2.40 ± 0.14	40.33 ± 4.70	0.43 ± 0.03*	2.80 ± 0.15
2 weeks	192.67 ± 12.24	41.00 ± 4.30	2.04 ± 0.10	24.25 ± 2.84	0.37 ± 0.03	2.88 ± 0.27
3 weeks	192.33 ± 13.54	47.33 ± 1.45	2.28 ± 0.15	29.00 ± 6.08	0.37 ± 0.03	2.80 ± 0.12

All parameters are expressed as average ± SE (n = 5).
The statistically significant differences were determined using one-way ANOVA.
* Clinically significant at $p < 0.05$.
** Highly significant at $p < 0.01$.
*** Extremely significant at $p < 0.001$.

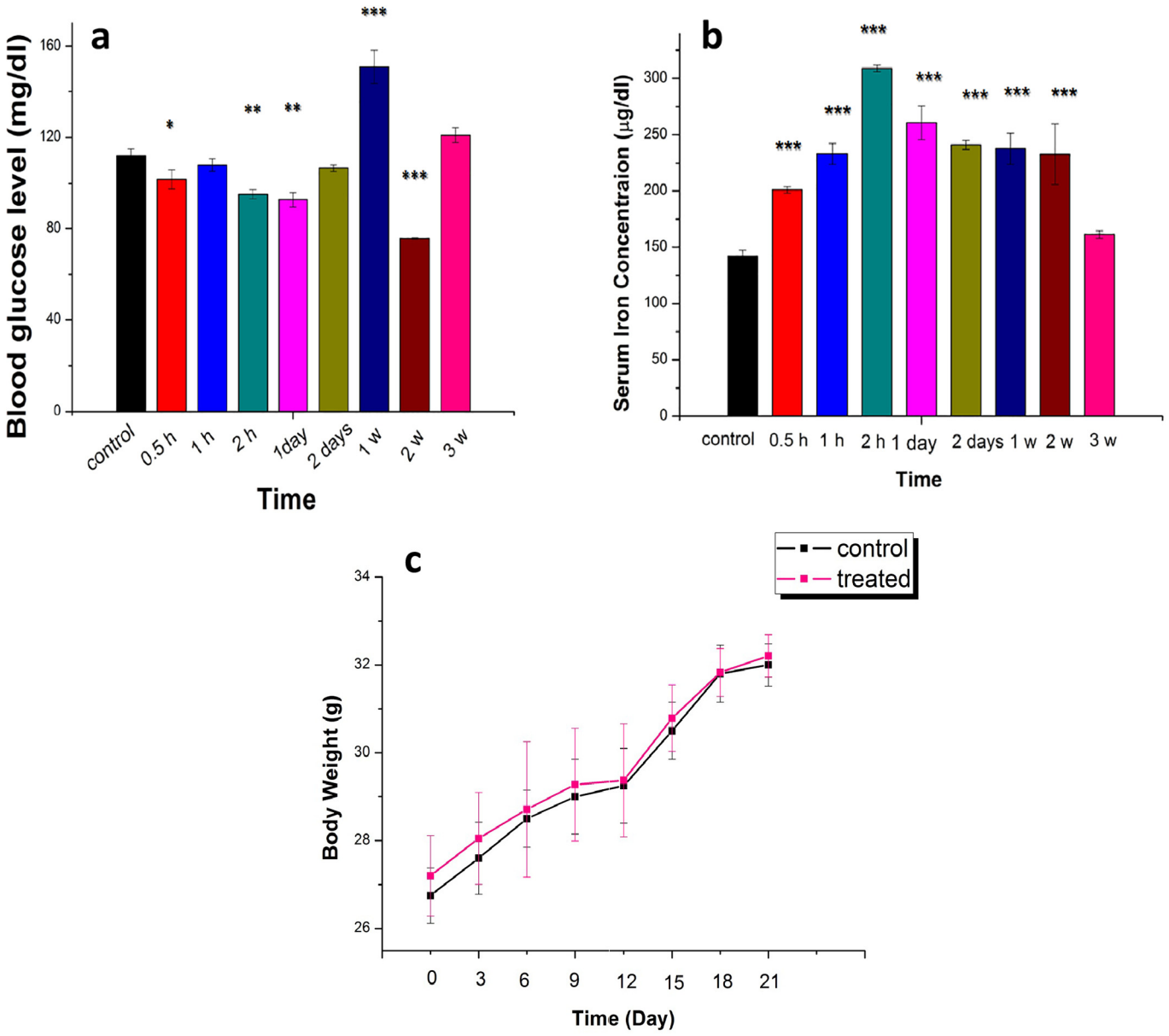

Fig. 4. (a) Blood glc level (mg/dl), (b) serum iron concentration (µg/dl) and (c) body weight for control group and Cur-IONPs treated group measured every 3 days throughout 3 weeks.

3.2.3. Body weight measurements

The body weight of the mice in both the treated and control groups showed no difference throughout the period of 3 weeks (Fig. 4c). Also, no abnormalities were observed in mice behaviour and activity. This is consistent with previous studies by Hanini et al. [49], Chamorro et al. [68] and Wei et al. [63] that showed a good general health for animals treated with IONPs as well as no obvious abnormal body weight loss or mortality in the treated mice.

The green synthesized IONPs with the golden medicinal spice curcumin exhibited superior properties that achieved biocompatibility (natural agent curcumin), non-toxicity and bio-safety.

Beyond the scope of the current study that addressed the biodistribution, clearness and toxicity of Cur-IONPs, we can suggest the potential utilization of Cur-IONPs in many biomedical applications:

i) As a drug nanocarrier that can be easily overcome the physiological limitations of drug transport especially the BBB [11,35].
ii) As a contrast agent in magnetic resonance imaging due to their superparamagnetic property and high cellular uptake (owing to their small size) [35,60].
iii) The curcumin coat is considered as a therapeutic agent against many diseases including neurological disorders and cancers.

Thus, Cur-IONPs is highly recommended as a biosafe candidate for the purposes of diagnosis and therapy “nanotheranostic”.

References

[1] S. Chinde, P. Grover, Toxicological assessment of nano and micron-sized tungsten oxide after 28days repeated oral administration to Wistar rats, Mutat. Res. 819 (2017) 1–13.
[2] L.W. Zhang, et al., Biological interactions of quantum dot nanoparticles in skin and in human epidermal keratinocytes, Toxicol. Appl. Pharmacol. 228 (2) (2008) 200–211.
[3] A. Verma, F. Stellacci, Effect of surface properties on nanoparticle–cell interactions, Small 6 (1) (2010) 12–21.
[4] A.D. Maynard, et al., Safe handling of nanotechnology, Nature 444 (7117) (2006) 267–269.
[5] A. Nel, et al., Toxic potential of materials at the nanolevel, Science 311 (5761) (2006) 622–627.

[6] M.N. Helmus, The need for rules and regulations, Nat. Nanotechnol. 2 (6) (2007) 333–334.
[7] N.V. Lewinski, et al., Cytotoxicity of nanoparticles, Small 4 (1) (2008) 26–49.
[8] S. Li, et al., Fluorescent nanoparticles present in Coca-Cola and Pepsi-Cola: physiochemical properties, cytotoxicity, biodistribution and digestion studies, Nanotoxicology 12 (1) (2018) 49–62.
[9] N. Khlebtsov, L. Dykman, Biodistribution and toxicity of engineered gold nanoparticles: a review of in vitro and in vivo studies, Chem. Soc. Rev. 40 (3) (2011) 1647–1671.
[10] N. Hoshyar, et al., The effect of nanoparticle size on in vivo pharmacokinetics and cellular interaction, Nanomedicine (Lond) 11 (6) (2016) 673–692.
[11] H. Nosrati, et al., Green and One-Pot Surface Coating of Iron Oxide Magnetic Nanoparticles with Natural Amino Acids and Biocompatibility Investigation, Organometallic Chemistry, (2017), pp. 1–10.
[12] H. Nosrati, et al., Methotrexate-conjugated L-lysine coated iron oxide magnetic nanoparticles for inhibition of MCF-7 breast cancer cells, Drug Dev. Ind. Pharm. 44 (6) (2018) 886–894.
[13] Jaiswal, et al., Biocompatibility, biodistribution and efficacy of magnetic nanohydrogels in inhibiting growth of tumors in experimental mice models, Biomater. Sci. 2 (2014) 370–380.
[14] Kumar, et al., In vivo biodistribution and clearance studies using multimodal organically modified silica nanoparticles, ACS.Nano 4 (2) (2010) 699–708.
[15] K.L. Aillon, et al., Effects of nanomaterial physicochemical properties on in vivo toxicity, Adv. Drug Deliv. Rev. 61 (6) (2009) 457–466.
[16] H.Y. Jia, et al., Potential oxidative stress of gold nanoparticles by induced-NO releasing in serum, J. Am. Chem. Soc. 131 (1) (2008) 40–41.
[17] Y. Pan, et al., Gold nanoparticles of diameter 1.4 nm trigger necrosis by oxidative stress and mitochondrial damage, Small 5 (18) (2009) 2067–2076.
[18] X. Liu, et al., Surface and size effects on cell interaction of gold nanoparticles with both phagocytic and nonphagocytic cells, Langmuir 29 (29) (2013) 9138–9148.
[19] C. Cruje, B.D. Chithrani, Integration of peptides for enhanced uptake of PEGylayed gold nanoparticles, J. Nanosci. Nanotechnol. 15 (3) (2015) 2125–2131.
[20] S.A. Kulkarni, S.S. Feng, Effects of particle size and surface modifcation on cellular uptake and biodistribution of polymeric nanoparticles for drug delivery, Pharm. Res. 30 (2013) 2512–2522.
[21] X. Sun, et al., An assessment of the effects of shell crosslinked nanoparticle size, core composition, and surface PEGylation on in vivo biodistribution, Biomacromolecules 6 (2005) 2541–2554.
[22] S.D. Perrault, et al., Mediating tumor targeting effciency of nanoparticles through design, Nano Lett. 9 (2009) 1909–1915.
[23] L. Dykman, N. Khlebtsov, Gold nanoparticles in biomedical applications: recent advances and perspectives, Chem. Soc. Rev. 41 (6) (2012) 2256–2282.
[24] A.M. Alkilany, C.J. Murphy, Toxicity and cellular uptake of gold nanoparticles: what we have learned so far? J. Nanopart. Res. 12 (7) (2010) 2313–2333.
[25] C. Uboldi, et al., Gold nanoparticles induce cytotoxicity in the alveolar type-II cell lines A549 and NCIH441, Part. Fibre Toxicol. 6 (1) (2009) 18.
[26] D. Pissuwan, et al., A solid-in-oil dispersion of gold nanorods can enhance transdermal protein delivery and skin vaccination, Small 7 (2) (2011) 215–220.
[27] L. Sun, D. Liu, Z. Wang, Functional gold nanoparticle− peptide complexes as cell-targeting agents, Langmuir 24 (18) (2008) 10293–10297.
[28] A.K. Gupta, M. Gupta, Synthesis and surface engineering of iron oxide nanoparticles for biomedical applications, Biomaterials 26 (18) (2005) 3995–4021.
[29] Sukhanova, et al., Dependence of nanoparticle toxicity on their physical and chemical properties, Nanoscale Res. Lett. 13 (44) (2018) 1–21.
[30] E.C. Dreaden, et al., Size matters: gold nanoparticles in targeted cancer drug delivery, Ther. Deliv. 3 (4) (2012) 457–478.
[31] N.S. Elbialy, M.M. Fathy, W.M. Khalil, Preparation and characterization of magnetic gold nanoparticles to be used as doxorubicin nanocarriers, Phys. Medi. Eur. J. Med. Phys. 30 (7) (2014) 843–848.
[32] N.S. Elbialy, M.M. Fathy, W.M. Khalil, Doxorubicin loaded magnetic gold nanoparticles for in vivo targeted drug delivery, Int. J. Pharm. 490 (1–2) (2015) 190–199.
[33] H. Ittrich, K. Peldschus, N. Raabe, et al., Superparamagnetic iron oxide nanoparticles in biomedicine: applications and developments in diagnostics and therapy, Fortschr Röntgenstr 185 (12) (2013) 1149–1166.
[34] A. Lindemann, K. Lüdtke-Buzug, B.M. Fräderich, et al., Biological impact of superparamagnetic iron oxide nanoparticles for magnetic particle imaging of head and neck cancer cells, Int. J. Nanomedicine 9 (2014) 5025–5040.
[35] H. Nosrati, et al., Glutathione (GSH) peptide conjugated magnetic nanoparticles as blood − brain barrier shuttle for MRI-monitored brain delivery of paclitaxel, ACS Biomater. Sci. Eng. 5 (2019) 1677 − 1685.
[36] A. Kunzmann, B. Andersson, C. Vogt, et al., Efficient internalization of silica-coated iron oxide nanoparticles of different sizes by primary human macrophages and dendritic cells, Toxicol. Appl. Pharmacol. 253 (2) (2011) 81–93.
[37] S.Y.R. Paik, J.S. Kim, S.J. Shin, et al., Characterization, quantification, and determination of the toxicity of iron oxide nanoparticles to the bone marrow cells, Int. J. Mol. Sci. 16 (9) (2015) 22243–22257.
[38] K. Tomankova, J. Horakova, M. Harvanova, et al., Cytotoxicity, cell uptake and microscopic analysis of titanium dioxide and silver nanoparticles in vitro, Food Chem. Toxicol. 82 (2015) 106–115.
[39] V. Valdiglesias, et al., Are iron oxide nanoparticles safe? Current knowledge and future perspectives, J. Trace Elem. Med. Biol. 38 (2016) 53–63.
[40] A. Albanese, P.S. Tang, W.C. Chan, The effect of nanoparticle size, shape, and surface chemistry on biological systems, Annu. Rev. Biomed. Eng. 14 (2012) 1–16.
[41] K.E. Sapsford, W.R. Algar, L. Berti, et al., Functionalizing nanoparticles with biological molecules: developing chemistries that facilitate nanotechnology, Chem. Rev. 113 (3) (2013) 1904–2074.
[42] K. El-Boubbou, Magnetic iron oxide nanoparticles as drug carriers: clinical relevance, Nanomedicine 13 (8) (2018) 953–971.
[43] R. Vijayakumar, V. Devi, K. Adavallan, et al., Green synthesis and characterization of gold nanoparticles using extract of anti-tumor potent Crocus sativus, Phys. E Low-Dimensional Syst. Nanostruct. 44 (3) (2011) 665–671.
[44] A. Zlotogorski, A. Dayan, D. Dayan, et al., Nutraceuticals as new treatment approaches for oral cancer–I: Curcumin, Oral Oncol. 49 (3) (2013) 187–191.
[45] C.A.C. Araujo, L.L. Leon, Biological activities of Curcuma longa L, Mem. Inst. Oswaldo Cruz 96 (5) (2001) 723–728.
[46] K. Quester, et al., SERS properties of different sized and shaped gold nanoparticles biosynthesized under different environmental conditions by Neurospora crassa extract, PLoS One 8 (10) (2013) 77486.
[47] P. Srivastava, et al., Synthesis of silver nanoparticles using haloarchaeal isolate Halococcus salifodinae BK 3, Extremophiles 17 (5) (2013) 821–831.
[48] R. Bhandari, P. Gupta, T.J. Dziubla, et al., Single step synthesis, characterization and applications of curcumin functionalized iron oxide magnetic nanoparticles, Mater. Sci. Eng. C 67 (2016) 59–64.
[49] A. Hanini, A. Schmitt, K. Kacem, et al., Evaluation of iron oxide nanoparticle biocompatibility, Int. J. Nanomedicine 6 (2011) 787–794.
[50] M. Ghorbani, et al., Curcumin-lipoic acid conjugate as a promising anticancer agent on the surface of gold-iron oxide nanocomposites: a pH-sensitive targeted drug delivery system for brain cancer theranostics, Eur. J. Pharm. Sci. 114 (2018) 175–188.
[51] A. Abbasi Kajani, A.-K. Bordbar, Biogenic magnetite nanoparticles: a potent and environmentally benign agent for efficient removal of azo dyes and phenolic contaminants from water, J. Hazard. Mater. 366 (2019) 268–274.
[52] A.M. Malekzadeh, A. Ramazani, R.S.J. Tabatabaei, et al., Design and construction of multifunctional hyperbranched polymers coated magnetite nanoparticles for both targeting magnetic resonance imaging and cancer therapy, J. Colloid Interface Sci. 490 (2017) 64–73.
[53] L. You, et al., Synthesis of multifunctional Fe3O4@PLGA-PEG nano-niosomes as a targeting carrier for treatment of cervical cancer, Mater. Sci. Eng. C 94 (2019) 291–302.
[54] L.C. Gonçalves, A.B. Seabra, M.T. Pelegrino, et al., Superparamagnetic iron oxide nanoparticles dispersed in Pluronic F127 hydrogel: potential uses in topical applications, RSC Adv. 7 (2017) 14496–14503.
[55] M. Saito, T. Matsuura, K. Nagatsuma, et al., The functional interrelationship between gap junctions and fenestrae in endothelial cells of the liver organoid, J. Membr. Biol. 217 (2007) 115–121.
[56] J. Wang, Y. Chen, B. Chen, et al., Pharmacokinetic parameters and tissue distribution of magnetic Fe3O4 nanoparticles in mice, Int. J. Nanomedicine 5 (2010) 861–866.
[57] M. Uchiyama, S. Toma, S. Rodrigues, et al., Ultrasmall cationic superparamagnetic iron oxide nanoparticles as nontoxic and efficient MRI contrast agent and magnetic-targeting tool, Int. J. Nanomedicine 10 (2015) 4731–4746.
[58] B.T.T. Pham, E.K. Colvin, T.H.P. Nguyen, et al., Biodistribution and clearance of stable superparamagnetic maghemite iron oxide nanoparticles in mice following intraperitoneal administration, Int. J. Mol. Sci. 19 (1) (2018) 205.
[59] L. Descamps, M.P. Dehouck, G. Torpier, et al., Receptor-mediated transcytosis of transferrin through blood-brain barrier endothelial cells, Am. J. Phys. 270 (1966) 1149–1158.
[60] H. Arami, A. Khandhar, D. Liggitt, et al., In vivo delivery, pharmacokinetics, biodistribution and toxicity of iron oxide nanoparticles, Chem. Soc. Rev. 44 (2015) 8576—8607.
[61] K.K. Cheng, P.S. Chan, S. Fan, et al., Curcumin-conjugated magnetic nanoparticles for detecting amyloid plaques in Alzheimer's disease mice using magnetic resonance imaging (MRI), Biomaterials 44 (2015) 155–172.
[62] E. Sadauskas, H. Wallin, M. Stoltenberg, et al., Kupffer cells are central in the removal of nanoparticles from the organism, Part. Fibre Toxicol. 4 (1) (2007) 1–7.
[63] Y. Wei, M. Zhao, F. Yang, et al., Iron overload by superparamagnetic iron oxide nanoparticles is a high risk factor in cirrhosis by a systems toxicology assessment, Sci. Rep. 6 (2016) 29110.
[64] P. Storey, R.P. Lim, H. Chandarana, et al., MRI assessment of hepatic iron clearance rates after USPIO administration in healthy adults, Investig. Radiol. 47 (2012) 717–724.
[65] X. Jiang, H. Dai, K.W. Leong, et al., Chitosan-g-PEG/DNA complexes deliver gene to the rat liver via intrabiliary and intraportal infusions, J. Gene Med. 8 (2006) 477–487.
[66] T.K. Jain, M.K. Reddy, M.A. Morales, et al., Biodistribution, clearance, and biocompatibility of iron oxide magnetic nanoparticles in rats, Mol. Pharm. 5 (2) (2008) 316–327.
[67] P. Bourrinet, H.H. Bengele, B. Bonnemain, et al., Preclinical safety and pharmacokinetic profile of ferumoxtran-10, an ultrasmall superparamagnetic iron oxide magnetic resonance contrast agent, Investig. Radiol. 41 (2006) 313–324.
[68] S. Chamorro, L. Gutiérrez, M.P. Vaquero, et al., Safety assessment of chronic oral exposure to iron oxide nanoparticles, Nanotechnology 26 (20) (2015) 205101.